Radiolabeled Phenethylguanidines:

Novel Imaging Agents for Cardiac Sympathetic Neurons and Adrenergic Tumors

David M. Raffel[*], **Yong-Woon Jung**, **David L. Gildersleeve**, **Phillip S. Sherman**, **James J. Moskwa**, **Louis J. Tluczek**, and **Wei Chen**
Division of Nuclear Medicine, Department of Radiology, 3480 Kresge III Building, University of Michigan Medical School, Ann Arbor, Michigan 48109

Abstract

The norepinephrine transporter (NET) substrates [^{123}I]*meta*-iodobenzylguanidine (MIBG) and [^{11}C]*meta*-hydroxyephedrine (HED) are used as markers of cardiac sympathetic neurons and adrenergic tumors (pheochromocytoma, neuroblastoma). However, their rapid NET transport rates limit their ability to provide accurate measurements of cardiac nerve density. [^{11}C]Phenethylguanidine ([^{11}C]**1a**) and 12 analogs ([^{11}C]**1b-m**) were synthesized and evaluated as radiotracers with improved kinetics for quantifying cardiac nerve density. In isolated rat hearts, neuronal uptake rates of [^{11}C]**1a-m** ranged from 0.24 to 1.96 mL/min/g wet, and six compounds had extremely long neuronal retention times (clearance $T_{1/2} > 20$ hr) due to efficient vesicular storage. PET studies in nonhuman primates with [^{11}C]**1e**, N-[^{11}C]guanyl-*meta*-octopamine, which has a slow NET transport rate, showed improved myocardial kinetics compared to HED. Compound [^{11}C]**1c**, [^{11}C]*para*-hydroxyphenethylguandine, which has a rapid NET transport rate, avidly accumulated into rat pheochromocytoma xenograft tumors in mice. These encouraging findings demonstrate that radiolabeled phenethylguanidines deserve further investigation as radiotracers of cardiac sympathetic innervation and adrenergic tumors.

Introduction

Radioiodinated *meta*-iodobenzylguanidine (MIBG, Figure 1) was originally developed by Wieland and coworkers as a radiotracer for scintigraphic imaging studies of adrenergic tumors such as neuroblastoma and pheochromocytoma.[1-3] As a structural analog of the neurotransmitter norepinephrine, MIBG concentrates in adrenergic tumors through active transport by the norepinephrine transporter (NET), which is richly expressed in the cell membranes of these tumors.[4-6] In addition to its successful application as a marker of adrenergic tumors, MIBG has proven to be very useful for scintigraphic imaging studies of cardiac sympathetic innervation.[7,8] MIBG is rapidly transported into cardiac sympathetic neurons by NET populations localized on the varicosities of terminal nerve axons.[9] Following uptake into the neuronal axoplasm, MIBG is transported into norepinephrine storage vesicles by the second isoform of the vesicular monoamine transporter (VMAT2),[7,10] the isoform expressed in peripheral sympathetic nerve terminals.[11]

With the advent of positron emission tomography (PET), several radiotracers labeled with positron-emitting radioisotopes were developed for PET studies of cardiac sympathetic innervation and adrenergic tumors. Early examples included the fluorine-18 labeled compounds 6-[^{18}F]fluorometaraminol[12] and 6-[^{18}F]fluorodopamine.[13] Following these were

[*]David M. Raffel, Ph.D., Division of Nuclear Medicine, Department of Radiology, 3480 Kresge III Building, University of Michigan Medical School, Ann Arbor, MI 48109-0552, USA, Telephone: (734) 936-0725, FAX: (734) 764-0288, Email: raffel@umich.edu

several carbon-11-labeled compounds, most in the form of N-[^{11}C]methyl-phenethylamines, including [^{11}C]*meta*-hydroxyephedrine ([^{11}C]HED, Figure 1)[14], [^{11}C]epinephrine ([^{11}C]EPI, Figure 1)[15] and [^{11}C]phenylephrine.[16] Positron-emitter-labeled analogs of MIBG have also been synthesized, including *meta*-[^{76}Br]bromobenzylguanidine[17] and *para*-[^{18}F] fluorobenzylguanidine.[18] While all of these compounds avidly localize in cardiac sympathetic neurons, there are significant differences in their neuronal handling in terms of NET transport rates, vulnerability to intraneuronal enzyme metabolism, efficiency of vesicular storage, and diffusion rates from neurons.[19]

[^{11}C]HED has been used extensively to study changes in cardiac sympathetic innervation in diabetic autonomic neuropathy, congestive heart failure, myocardial infarction, cardiac arrhythmias, and heart transplant patients.[20] The ability to assess the integrity of cardiac sympathetic innervation with radiotracers like [^{11}C]HED provides clinicians with valuable insights into a critical component of cardiac function. The physiologic information gained from these studies complements more traditional nuclear cardiology assessments of myocardial perfusion and myocardial viability.

While studies with the current generation of sympathetic nerve radiotracers have provided a wealth of information, all of these tracers share one common drawback: their uptake rates into cardiac sympathetic neurons are too rapid to allow for robust and reliable compartmental modeling of their kinetics. The inability to use kinetic modeling methods limits the quantitative information that can be garnered from clinical studies with these tracers. This situation is illustrated for [^{11}C]HED in Figure 2A. Following its delivery from plasma into the extracellular space (K_1), [^{11}C]HED is very rapidly taken up into sympathetic neurons by NET transport (k_3). The rapid neuronal uptake of [^{11}C]HED by NET transport (k_3) is much faster than clearance of the tracer from the extracellular space back to plasma (k_2), such that $k_3 \gg k_2$. Because neuronal uptake is much faster than clearance back to plasma, uptake of [^{11}C]HED into cardiac sympathetic neurons is rate-limited by delivery of the tracer from plasma to interstitium (K_1), rather than by NET transport (k_3). While it is evident from the shape of the myocardial kinetics of [^{11}C]HED that its neuronal uptake by NET transport is a fast process, it is so fast that there is insufficient information in the measured kinetics to precisely estimate the value of k_3 using kinetic modeling methods. This forces the use of semi-quantitative measurements of tracer retention instead of the more quantitative information provided by tracer kinetic modeling.[19,20] However, since neuronal uptake by NET transport (k_3) is much faster than clearance from interstitium back into plasma (k_2), [^{11}C]HED retention measurements are insensitive to low-to-moderate losses in NET density (i.e., nerve density), and decline only in myocardial regions in which nerve losses are severe.[21] Thus not only does the rapid neuronal uptake rate of [^{11}C]HED prevent successful tracer kinetic modeling of its myocardial kinetics, but it also tends to make measurements of its cardiac retention insensitive to low-to-moderate levels of nerve loss.

We hypothesized that this roadblock to accurate quantification could be overcome by developing a new radiotracer with inherently superior kinetic properties (Figure 2B). Specifically we hypothesized that a cardiac sympathetic nerve tracer would need to possess two kinetic properties to be ideal for quantitative analyses: (1) a slower neuronal uptake rate than current tracers such as [^{11}C]HED; and (2) a very long neuronal retention time, through trapping inside norepinephrine storage vesicles. The first criterion makes the neuronal uptake rate of the tracer rate-limited by NET transport (k_3) rather than by delivery from plasma to interstitium (K_1), by establishing conditions in which NET transport is slower than clearance from interstitium back into plasma ($k_3 < k_2$). A slower NET transport rate would allow some clearance of the tracer from tissue back into plasma after its initial extraction, greatly improving the ability of compartmental modeling techniques to make an accurate estimate of the neuronal uptake rate k_3 from the observed myocardial kinetics. In addition, it would make measurements

of tracer retention more sensitive to early losses in nerve density, allowing earlier detection of cardiac denervation in diseases. The second criterion has two purposes. First, since NET transport of the new tracer would be slower than for previous tracers, if the tracer was also efficiently trapped intraneuronally this would maximize the amount of radioactivity retained in the neurons, increasing image quality and providing better counting statistics for kinetic modeling efforts. Second, complete trapping of the tracer in the neuron following its neuronal uptake permits a simplification in the compartmental model structure, reducing the number of model parameters that need to be estimated from the kinetic data. This is important for PET studies where kinetic models with more than three or four rate constants are unfeasible. In this case, a 'trapped' neuronal tracer could be analyzed with the simplified compartment model shown in Figure 2C. The estimated value of k_3 in this simplified model would be a direct estimate of the neuronal transport rate of the radiotracer. Since neuronal transport rate by NET is highly sensitive to changes in nerve density, accurate estimates of this rate constant would effectively provide quantitative regional estimates of cardiac sympathetic nerve density. Such a tracer would represent a major advance in this branch of nuclear cardiology since it could be used to provide truly quantitative measures of regional nerve density. These measures would be more accurate and sensitive than the semi-quantitative measures of tracer retention used for the current generation of sympathetic nerve tracers.

Since vesicular storage is the mechanism we chose to exploit as a means of trapping a kinetically 'ideal' radiotracer inside sympathetic neurons, we decided to investigate radiolabeled phenethylguanidines as a potential class of compounds with high vesicular retention. Many phenethylguanidines are known to be potent depletors of cardiac norepinephrine stores *in vivo*, due to their avid uptake and retention inside norepinephrine storage vesicles.[22,23] In addition, phenethylguanidines have been shown to be more potent depletors of cardiac norepinephrine stores than benzylguanidines.[24] Although radiolabeled benzylguanidines such as [^{123}I]MIBG have been extensively studied as sympathetic nerve imaging agents, very little work has been done with radiolabeled phenethylguanidines. With these points in mind, we synthesized and evaluated a series of [^{11}C]phenethylguanidines as potentially 'optimal' imaging agents for PET studies of cardiac innervation (Figure 3).

Although these studies employed carbon-11 as the radiolabel, some of the phenethylguanidine structures evaluated included compounds with a ring fluoro- or iodo- group, with the idea that a successful compound could ultimately be synthesized with its corresponding radioisotope (i.e., replacing ring fluoro- with fluorine-18 for PET imaging or ring iodo- with iodine-123 for SPECT imaging). While it possible that changing the radiolabel from carbon-11 in the guanidine group of the side chain to a ring fluorine-18 or iodine-123 would lead to changes in the specific radiolabeled metabolites formed during an imaging study, we believe the *in vivo* kinetics of the ^{18}F-labeled or ^{123}I-labeled parent compounds would be very similar to those seen for their corresponding ^{11}C-labeled phenethylguanidines.

For cardiac PET imaging studies, carbon-11 and fluorine-18 are both good choices for the radiolabel. Carbon-11 maybe offer some advantages in terms of being able to inject two to three times more activity into a patient due to more favorable radiation dosimetry over fluorine-18. This provides higher tissue and blood concentrations of the tracer early in the study, when the kinetics of the tracer are changing most rapidly. In addition, the radiosynthetic methods to prepare the carbon-11 compound are much simpler and faster than those required to prepare a fluorine-18 compound. However, the use of carbon-11 requires that a PET center have an onsite cyclotron and staff to prepare the radiopharmaceutical. A successful fluorine-18 labeled compound could be prepared by commercial vendors and distributed to stand-alone PET centers for cardiac and cancer imaging studies, much as the glucose analog 2-[^{18}F] fluoro-2-deoxy-glucose (FDG) is distributed today. In terms of the kinetics of these tracers however, it should be emphasized that we are not attempting to measure the overall clearance

rates of these compounds from the heart, so it is not necessary to use a radiolabel with a longer half-life than carbon-11. The main goal of developing a radiotracer with a slower NET transport rate and very long neuronal retention time is to bestow the tracer with kinetic properties that allow its neuronal uptake rate k_3 to be accurately estimated from the myocardial kinetics measured during a 60 min PET study.

Finally, in addition to the main goal of developing an optimal PET tracer for quantitative studies of cardiac sympathetic innervation, a secondary goal was to test the ability of $[^{11}C]$ phenethylguanidines to act as imaging agents for localization of adrenergic tumors.

Results and Discussion

Chemistry

Phenethylguanidines **1a-m** were synthesized for HPLC standards and *in vitro* studies (Scheme 1). Most of the primary amine precursors **2a-m** were available commercially, but 4-fluoro- and 6-fluoro-3-hydroxyphenethylamines (**2j, 2k**) were prepared in multiple steps from 4-fluoro- or 6-fluoro-3-methoxybenzaldehyde utilizing previously published methods[25]. Two established methods were used to prepare **1a-m** (Scheme 1). Method A, the Rathke Reaction[26,27] involves nucleophilic attack by the phenethylamine precursor on the amidine derivative 2-methyl-2-thiopseudourea to yield the phenethylguanidine, which was subsequently purified by recrystallization. Method B is a two-step reaction: condensation of the phenethylamine precursor with 1,3-bis(benzyloxycarbonyl)-2-methyl-2-thiopseudourea [28] is followed by hydrogenolysis over Pd/C to afford the phenethylguanidine. Although the Rathke Reaction is a straightforward one-step reaction, some phenethylguanidines could not be purified by recrystallization due to poor separation from the reactant 2-methyl-2-thiopseudourea and phenethylamine precursors. We successfully used the Rathke method to synthesize most compounds (**1a, 1c-i**). Chemical yields were 32-93% and chemical purities were >98% after several recrystalizations from ethanol in water. Method B was used to synthesize the remaining phenethylguanidines (**1b, 1j, 1k**). Chemical yields were 63-82% and chemical purities were >95%. Chemical purities were determined using high performance liquid chromatography (HPLC) with UV detection (241 nm).

Radiochemistry

$[^{11}C]$phenethylguanidines ($[^{11}C]$**1a-m**) were synthesized from $[^{11}C]$CNBr using methods developed by Westerberg and Långström[29] with a few modifications (Scheme 2). The phenethylamine precursor (**2a-m**; 1.0-1.5 mg), as the free base or hydrochloride salt, dissolved in 0.25 mL of borate buffer (pH 8.0), was reacted with $[^{11}C]$CNBr to produce the $[^{11}C]$ cyanamide intermediate $[^{11}C]$**4a-m**, followed by treatment with ammonia to yield $[^{11}C]$**1a-m**. The product was purified by reversed-phase HPLC. Corrected radiochemical yields were 2.5-6% (relative to $[^{11}C]$CO$_2$ produced), with specific activities of >500 Ci/mmol at end-of-synthesis (EOS). Radiochemical and chemical purities were >98%. For most compounds, 25 - 60 mCi of the $[^{11}C]$phenethylguanidine was obtained at EOS.

Kinetic Studies in Isolated Rat Heart

Uptake rates of $[^{11}C]$**1a-m** into sympathetic neurons, as well as the ability of cardiac neurons to retain these compounds, were assessed by performing kinetic studies in an isolated working rat heart preparation. In all of these studies, the extraneuronal catecholamine uptake mechanism in the rat heart ('uptake-2') was inhibited by adding 54 μM corticosterone to all heart perfusion buffers.[30] Neuronal uptake rates (K_{up}; mL/min/g wet) were measured by performing a 10 min infusion of the radiotracer at a constant perfusate concentration into the isolated heart. At the end of the constant infusion period, the heart was switched to normal perfusion buffer for 120 min to measure radiotracer clearance rates (expressed as a half-time, $T_{1/2}$, in hr). Neuronal

uptake rates for [¹¹C]**1a-m** varied widely, ranging from 0.24 mL/min/g wet for [¹¹C]**1g** to 1.96 mL/min/g wet for [¹¹C]**1b** (Table 1). These are all slower than the previously measured neuronal uptake rates of 2.66 mL/min/g wet for [¹¹C]HED[31] and 3.66 mL/min/g wet for [¹²³I]MIBG.[9] However, some were faster than the reported rate of 0.66 mL/min/g wet for [¹¹C]EPI[32], suggesting that compounds with neuronal uptake rates lower than this value may be the ones best suited for kinetic modeling in cardiac PET studies. Clearance rates fell into one of two groups, those with relatively fast clearance (clearance $T_{1/2}$ = 1.9 - 4.4 hr) and those with extremely long neuronal retention (clearance $T_{1/2}$ > 20 hr). These clearance rates can be compared to values of 1.1 hr for [¹¹C]HED[31] and 1.9 hr for [¹²³I]MIBG[9], while retention of [¹¹C]EPI in the isolated rat heart also is extremely long.[32] Six of the of the 13 phenethylguanidine structures exhibited the desired kinetic property of a very long neuronal retention time (Figure 4A). These six compounds share a common structural feature of having at least one hydroxyl substitution in either the phenyl ring or the β-carbon of the side chain. In fact, from examination of Table 1 it can be seen that the six compounds with at least one hydroxyl substitution all had very long neuronal retention times, while the remaining compounds lacking a hydroxyl substitution had faster clearance rates. Thus it appears that a minimum structural requirement for long neuronal retention is a β-carbon or phenyl ring hydroxyl group substitution. It has been shown that phenethylamines must possess at least two hydroxyl groups to be tightly bound inside the storage vesicles of cardiac sympathetic neurons.[33] Thus it appears that the highly polar N-[¹¹C]guanyl group of these [¹¹C] phenethylguanidines is acting like a hydroxyl group in terms of contributing to high vesicular uptake and retention, such that the addition of a single hydroxyl group to the phenethylguanidine structure is sufficient to ensure prolonged vesicular retention.

The main effect of ring hydroxylation at the *meta* or *para* position was to extend neuronal retention times. For example, comparing [¹¹C]**1b** and [¹¹C]**1c** to the unsubstituted reference compound [¹¹C]**1a**, there was modest effects on neuronal uptake rate but neuronal retention times were greatly prolonged. Similarly, comparing [¹¹C]**1d** with its *meta*-hydroxylated analog [¹¹C]**1e**, little difference in the neuronal uptake rates was seen but [¹¹C]**1e** had a much longer retention time. Adding a *meta*-hydroxy group to [¹¹C]**1h** and [¹¹C]**1i** to form [¹¹C]**1j** and [¹¹C]**1k**, respectively, also led to greatly extended neuronal retention times. However, [¹¹C]**1k** did have a significantly slower neuronal uptake rate than [¹¹C]**1i**, so in some cases ring hydroxylation does appear to affect the neuronal uptake rate.

Ring fluoro- substitutions affected both neuronal uptake rates and clearance rates. The neuronal uptake and clearance kinetics of the unsubstituted reference compound [¹¹C]**1a** and its *ortho*-fluoro ([¹¹C]**1i**), *para*-fluoro ([¹¹C]**1h**) and *meta*-fluoro ([¹¹C]**1g**) analogs are shown in Figure 4B. While these compounds did not exhibit the desired long neuronal retention for cardiac applications, it is possible that one of these compounds, if labeled with fluorine-18, could be useful for detection of adrenergic tumors using PET. The radiolabeled benzylguanidine *para*-[¹⁸F]fluorobenzylguanidine ([¹⁸F]PFBG) has previously been shown to be capable of detecting pheochromocytomas with PET.[34] In the isolated rat heart, [¹⁸F]PFBG has a neuronal uptake rate of 1.2 mL/min/g wet and a clearance $T_{1/2}$ of 0.53 hr.[35] Thus, the fluorine-18 analog of compound [¹¹C]**1i**, which has a faster neuronal uptake rate (1.76 mL/min/g wet) and slower clearance rate ($T_{1/2}$ = 2.3 hr) than [¹⁸F]PFBG, could potentially be useful as a PET imaging agent for localizing adrenergic tumors.

The *meta*-iodo ([¹¹C]**1l**) and *para*-iodo ([¹¹C]**1m**) compounds had slower neuronal uptake rates and faster clearance rates than the unsubstituted reference compound [¹¹C]**1a**. Both compounds have neuronal uptake rates that are slower than the rate measured for the clinically used compound [¹²³I]MIBG (3.66 mL/min/g wet), but have clearance rates comparable to the 1.9 hr value measured for [¹²³I]MIBG.[9] The perfusate concentrations of [¹¹C]**1l** and [¹¹C] **1m** were < 10 nM, which is five times lower than the K_m for NET transport of [¹²³I]MIBG (52

nM) in the isolated rat heart[36], so we believe our measurements with these compounds can be directly compared to the reported values for [^{123}I]MIBG without concerns of specific activity effects. The slower neuronal uptake rate of these iodo-phenethylguanidines may make their cardiac retention in human heart more sensitive to low-to-moderate degrees of cardiac denervation than [^{123}I]MIBG, since their neuronal uptake is less likely to be rate-limited by delivery from plasma. Thus an ^{123}I-labeled analog of either compound [^{11}C]**1l** or [^{11}C]**1m** may prove to be clinically useful for assessing cardiac sympathetic innervation with SPECT imaging.

To verify that vesicular storage is the mechanism responsible for the prolonged neuronal retention of some [^{11}C]phenethylguanidines, the neuronal uptake and retention of [^{11}C]**1c** was measured in a heart isolated from a rat treated with the potent VMAT2 inhibitor reserpine (1 mg/kg *i.p.*, 3 hr before heart isolation). Blocking vesicular uptake of [^{11}C]**1c** with reserpine greatly reduced retention of the compound, both by reducing tracer accumulation into neurons during the constant infusion period and by accelerating the clearance rate during the washout phase of the study (Figure 5). Thus vesicular storage is a very important process that increases the tracer's neuronal distribution volume and prolongs tracer retention. To test whether significant leakage of [^{11}C]**1c** occurs from vesicles and nerve terminals during the clearance phase of the study, with neuronal reuptake by NET as a potential mechanism for prolonging its neuronal retention, a pharmacological 'chase' study was performed. The high affinity NET inhibitor desipramine (DMI) was added to the heart perfusion buffer for the clearance phase of the study. As seen in Figure 5, DMI chase not only did not accelerate the clearance of [^{11}C]**1c** from the nerves, consistent with the view that the compound remains largely sequestered inside storage vesicles, but instead prevented any measurable release of [^{11}C]**1c** from the nerve terminals. The observation that DMI chase acted to completely abolish neuronal clearance suggests that the primary mechanism of [^{11}C]**1c** clearance from nerves in the isolated rat heart is through NET transport acting in reverse, rather than through passive diffusion.

To test the hypothesis that [^{11}C]phenethylguanidines are more avidly taken up and retained by storage vesicles than [^{11}C]benzylguanidines, we prepared [^{11}C]**5**, [^{11}C]*para*-hydroxybenzylguanidine (PHBG), the benzylguanidine analog of compound [^{11}C]**1c**. The kinetics of [^{11}C]**5** in the isolated rat heart are shown in Figure 6, in comparison with those of [^{11}C]**1c**. [^{11}C]**5** had a slower neuronal uptake rate than [^{11}C]**1c** (K_{up} = 0.93 mL/min/g wet) and a much faster clearance time ($T_{1/2}$ = 1.2 hr). Although this finding is only for a single structural pair, the striking difference in the neuronal retention times of these two compounds suggests that some phenethylguanidines are better substrates for vesicular uptake by VMAT2 than their benzylguanidines analogs.

Biodistribution Studies in Rats

For the six [^{11}C]phenethylguanidines that exhibited very long neuronal retention times in the isolated rat heart, *in vivo* biodistribution studies were performed in rats (Table 2). Tissue concentrations of the radiotracer were determined 30 min after intravenous injection, and expressed as a percentage of the injected dose per g of tissue (%ID/g). For comparison, biodistribution studies were also performed for [^{11}C]HED and [^{11}C]EPI. These data provide some indications of the suitability of a compound as an imaging agent for human studies. For example, for cardiac imaging studies, low uptake in the liver and lungs are desirable since they are in close proximity to the heart. Similarly, high heart-to-blood ratios are desirable as they provide high quality images of the heart wall, which aids in the interpretation of abnormalities in tracer retention. For the compounds studied, *in vivo* uptake into the left ventricle (LV) tended to be linearly correlated with the neuronal uptake rate in the isolated rat heart, K_{up}. A correlation coefficient r^2 = 0.57 ($P < 0.03$) was found between *in vivo* tissue concentrations in the LV at 30 min and K_{up} values measured in the isolated rat heart (Figure 7A). Normalizing LV

concentrations to corresponding blood concentrations for each compound, calculated LV/blood ratios at 30 min were also found to be linearly correlated with K_{up} ($r^2 = 0.74$; $P < 0.006$; Figure 7B). These results show that, in the rat heart, measured neuronal uptake rates in the isolated rat heart are predictive of *in vivo* LV uptake and LV/blood ratios.

Note that extraneuronal uptake (uptake-2) was not inhibited in these biodistribution studies, so an undetermined fraction of the measured LV uptake at 30 min is due to extraneuronal uptake into myocytes. [11C]HED is a very poor substrate of uptake-2,[31] and more than 92% of its LV uptake at 30 min is intraneuronal.[14] In microPET imaging studies of compound [11C]**1c** in rats ($n = 2$), after myocardial uptake levels peaked at around $T = 5$ min, 21-25% of compound cleared from the heart down to a plateau of activity at the end of the 60 min study. Given the efficient intraneuronal trapping of [11C]**1c** in the isolated rat heart (Table 1), and previous demonstrations of fast clearance of [123I]MIBG[9] and [76Br]MBBG[37] from the extraneuronal compartment of the rat heart, this relatively fast clearance component is likely associated with extraneuronal uptake. At $T = 30$ min, we estimate that 92-95% of [11C]**1c** in the heart was intraneuronal. For compounds with lower neuronal uptake rates (K_{up}) in the isolated rat heart, the fraction of LV uptake at $T = 30$ min shown in Table 2 that is associated with extraneuronal uptake may be higher than for [11C]**1c**. However, the good correlation between neuronal uptake rates measured with uptake-2 blocked in the isolated rat heart and *in vivo* retention in the rat heart suggests that most of the measured LV uptake for these compounds was inside neurons.

In terms of liver uptake, compounds with a hydroxyl group at the β-carbon position of the side chain ([11C]HED, [11C]EPI, [11C]**1d** and [11C]**1e**) all had substantially higher liver uptake than compounds without a β-carbon hydroxyl group ([11C]**1b**, [11C]**1c**, [11C]**1j** and [11C]**1k**). This suggests that compounds without a β-carbon hydroxyl group would be preferable for cardiac innervation and adrenergic tumor imaging studies, since high uptake of radiotracers into the liver can be problematic for both of these imaging procedures.

In a previous study of [11C]HED uptake in rats, Law et al. demonstrated that tissue uptake of [11C]HED was proportional to injected dose for intravenous injections containing less than 8 nmol/kg of total HED mass[38]. For all of the biodistribution studies shown in Table 2, the injected doses of the compounds were less than 1 nmol/kg. Using the [11C]HED data as a guide, we believe that the specific activities of the compounds studied were high enough that mass effects did not cause decreases in the measured tissue uptake values.

MicroPET Imaging Studies: Cardiac Imaging in Monkeys

The hearts of monkeys[39] and humans[40,41] lack the extraneuronal uptake (uptake-2) pathway of catecholamines, making the monkey a more appropriate animal model for evaluating sympathetic nerve tracers than the dog, which has robust uptake-2 activity[42]. Cardiac imaging studies of two [11C]phenethylguanidines, [11C]**1b** and [11C]**1e**, were performed in rhesus macaque monkeys to assess their *in vivo* kinetics and imaging properties. These two compounds had the fastest and the slowest neuronal uptake rates in the isolated rat heart, respectively. For comparison, [11C]HED was also studied. The imaging properties and myocardial kinetics of [11C]HED ($n = 3$; Figure 8A) were very similar to what is observed in cardiac PET studies in normal human subjects[43], suggesting that the rhesus macaque monkey is an excellent animal model for preclinical testing of cardiac sympathetic nerve tracers. Uptake of [11C]HED into cardiac sympathetic nerves was very rapid, with myocardial tissue concentrations of [11C]HED staying nearly constant for the remainder of the 60 min imaging study. Heart-to-blood ratios averaged 4.5 ± 0.2 at the end of the study, providing high quality images with good contrast between the LV wall and blood in the LV chamber. Final heart-to-liver ratios were 1.9 ± 0.1. The myocardial kinetics of [11C]**1e** were substantially different from those of [11C]HED ($n = 3$; Figure 8B). Heart activity peaked shortly after intravenous injection of the tracer, followed by a rapid decline of activity, evidence that some of the tracer extracted from the plasma into

the tissue compartments cleared back out into the bloodstream. After this, a steady accumulation of the compound into cardiac sympathetic nerves occurred, leading to myocardial tissue concentrations at the end of the study that were ~ 73% of the final concentrations seen with [^{11}C]HED. The relatively high final tissue concentrations of [^{11}C]**1e** that were achieved are remarkable considering that this compound has a neuronal uptake rate in the isolated rat heart (K_{up}) that is only one-ninth the rate of [^{11}C]HED. This indicates that unlike the situation in the rat heart *in vivo*, neuronal uptake rates measured for these compounds in the isolated perfused rat heart are not necessarily good predictors of final LV concentrations in the hearts of non-human primates. Furthermore, the shape of the time-activity curve for [^{11}C]**1e** in monkey heart is very encouraging in terms of applying tracer kinetic modeling methods. Clearance of some of the tracer that is initially extracted into the tissue back out into the bloodstream is a hallmark of a tracer that is not rate-limited by delivery from plasma to tissue, but instead is rate-limited by neuronal uptake by NET transport. Also, the steady accumulation of the compound during the study is consistent with trapping inside storage vesicles within neurons. Thus the myocardial kinetics of [^{11}C]**1e** appear to be much better suited for quantifying regional nerve density in the heart using tracer kinetic modeling techniques than [^{11}C]HED. Further studies with this promising compound, including tracer kinetic modeling of its myocardial kinetics in the monkey, are ongoing. The one drawback with [^{11}C]**1e** is the relatively high liver uptake that was seen; final heart-to-liver ratios were 0.6 ± 0.1. This high liver uptake is consistent with what was observed *in vivo* in the rat biodistribution studies, and appears to be due to the β-hydroxyl group. Finally, the myocardial kinetics of [^{11}C]**1b** were very similar to those of [^{11}C]HED ($n = 1$; Figure 8C). Again, there was very rapid neuronal uptake of the compound early in the study, with nearly constant retention for the duration of the PET scan, with a final heart-to-blood ratio of ~ 4.7. However, of the three compounds studied, [^{11}C]**1b** had the lowest liver uptake, resulting in a heart-to-liver ratio of ~ 4.4 and providing the highest quality images. This is the only compound of the three lacking a hydroxyl group on the β-carbon position, again supporting the view that it is this structural feature that causes high liver uptake. Despite the higher quality of the images with [^{11}C]**1b** as compared with [^{11}C]HED, since both of these compounds appear to have their neuronal uptake rate-limited by delivery from plasma to tissue, from a kinetic modeling viewpoint this tracer would not offer any advantages over [^{11}C]HED. These initial imaging studies suggest that a phenethylguanidine structure possessing *in vivo* kinetics similar to [^{11}C]**1e** but lacking a β-carbon hydroxyl group to reduce liver uptake would have optimal kinetics and imaging properties for quantitative PET studies of cardiac sympathetic innervation.

MicroPET Imaging Studies: Tumor Imaging in Mice

While a slower NET transport rate is better for quantitative PET studies of cardiac innervation, rapid NET transport is a desirable tracer kinetic property for imaging studies of adrenergic tumors. In addition, long retention times inside tumors can lead to high tumor-to-background ratios, improving imaging conditions for tumor localization. Two of the compounds tested in the isolated rat heart had both a rapid NET transport rate and very long retention inside cardiac neurons, [^{11}C]**1b** and [^{11}C]**1c**. Since the rat biodistribution data suggested that LV uptake and blood levels of [^{11}C]**1c** were higher than those of [^{11}C]**1b**, but with comparable liver uptake, we chose to test the ability of [^{11}C]**1c** to localize adrenergic tumors in a mouse model. [^{11}C]**1c** was avidly taken up by pheochromocytoma (PC12) xenografts implanted in the left flank of Balb/c *nu/nu* nude mice (Figure 9). Tumor uptake of [^{11}C]**1c** reached peak levels of ~29 % ID/g tissue within 10 min and stayed constant out to 60 min. By comparison, heart uptake at 60 min was ~17 %ID/g tissue. In addition, uptake into background tissues such as the liver, lungs and gut were very low. Low background radioactivity in these structures is advantageous since it increases tumor-to-background ratios in these areas. When tumor localization studies are performed with radiolabeled MIBG, a delay of at least 24 hr is imposed to improve tumor-to-background ratios, and in some cases residual uptake in the liver makes tumor localization

challenging.[44] Thus a tracer that rapidly localizes in adrenergic tumors in less than one hour, with very low uptake in the liver, gut, and other tissues would represent a significant improvement over MIBG. These encouraging initial findings suggest that [^{11}C]**1c** or another radiolabeled phenethylguanidine with rapid NET transport and long retention in tumors would be very useful for localizing adrenergic tumors.

Conclusion

In summary, we synthesized and evaluated a series of [^{11}C]phenethylguanidines as potential PET and SPECT imaging agents for quantitative studies of cardiac sympathetic innervation or as diagnostic imaging agents for adrenergic tumors. Studies in the isolated working rat heart demonstrated that [^{11}C]phenethylguanidine structures with at least one hydroxyl group substitution in the phenyl ring or the β-carbon position of the side chain had extremely long intraneuronal retention times due to avid accumulation and retention inside storage vesicles. In PET imaging studies in nonhuman primates, compound [^{11}C]**1e** had greatly improved myocardial kinetics for quantitative tracer kinetic analyses over the currently used PET tracer [^{11}C]HED. PET imaging studies in mice implanted with pheochromocytoma tumors showed that compound [^{11}C]**1c** was avidly taken up by the tumors while tracer uptake into background tissues such as liver, lung and gut were very low. We believe these encouraging initial findings with radiolabeled phenethylguanidines demonstrate that further development of these novel imaging agents is warranted, including the evaluation of new structures and a more thorough characterization of the *in vivo* kinetics of the most promising compounds.

Experimental Section

^{1}H NMR spectra were recorded on a Varian Inova instruments operating at 400 MHz or 300 MHz, respectively. Chemical shifts (δ) are given in parts per million (ppm) relative to internal standard tetramethylsilane (TMS) and coupling constants (*J*) are in Hz. High-resolution mass spectra were obtained on a VG-250S spectrometer using electrospray ionization (ESI) in positive ion mode, direct chemical ionization (DCI) or electron impact (EI) at 70 eV. Melting points were determined on a Thomas-Hoover capillary melting point apparatus in open capillary tubes and are uncorrected. Flash chromatography utilized Merck 230-400 mesh silica gel. Thin-layer chromatography (TLC) used Analtech 0.25 mm glass-backed plates with fluorescent background. Visualization was achieved by phosphomolybdic acid (PMA) or UV illumination. High pressure liquid chromatography (HPLC) was performed on a Hitachi pump L-7100 instrument equipped with Hitachi D-7500 integrator and Hitachi L-4000 UV detector. Radioactivity detection was done with Bioscan coincidence (model B-FC-4000) detector.

Reagents and solvents were purchased from commercial sources and used without further purification unless otherwise noted. Samples of 3-iodophenethylguanidine sulfate (MIPG) and 4-iodophenethylguanidine sulfate (PIPG) previously prepared in our laboratory were used as HPLC standards.[3]

General Procedure for the Rathke Reaction

A two-necked flask was equipped with an N_2 inlet tube and a reflux condenser. The end of the condenser was fitted with an N_2 exit tube connected successively to an empty backup trap, a second trap containing 25% aq. NaOH and a third trap containing 5% aq. NaOCl. A mixture of phenethylamine precursor (10.0 mmol) and 2-methyl-2-thiopseudourea sulfate (5.0 mmol) in water-ethanol (24 mL, 1:1 v/v) was heated under reflux with a slow stream of N_2 passing through the liquid to entrain CH_3SH, until the reaction was complete. The solvent was evaporated under reduced pressure to give the solid or viscous oil product. The crude product was washed with ether (2×30 mL), recrystallized two or three times with an appropriate solvent and dried *in vacuo* to afford the pure phenethylguanidine analog.

Phenethylguanidine sulfate (1a)

93% yield after recrystallization from water: mp 168-171°C (lit.45 168-173°C); ^{1}H NMR (400 MHz, CD$_3$OD): δ 2.88 (t, J = 7.5 Hz, 2H), 3.39 (t, J = 7.5 Hz, 2H), 7.19-7.31 (m, 5H); HRMS calcd for C$_9$H$_{13}$N$_3$ 163.1109 (M$^+$), obsd 163.1103.

4-Hydroxyphenethylguanidine sulfate (1c)

85% yield after recrystallization from ethanol: mp 243-247°C (lit.46 245-250°C); ^{1}H NMR (400 MHz, CD$_3$OD): δ 2.77 (t, J = 7.3 Hz, 2H), 3.34 (t, J = 7.3 Hz, 2H), 6.72 (d, J = 8.6 Hz, 2H), 7.07 (d, J = 8.6 Hz, 2H); HRMS calcd for C$_9$H$_{13}$N$_3$O 180.1137 (M + H)$^+$, obsd 180.1131.

(-)-β-Hydroxyphenethylguanidine sulfate (1d)

52% yield after recrystallization from ethanol/water: mp 229-231°C (lit.23 228°C); $[\alpha]_D^{23}$ -36° in 50% aqueous MeOH; ^{1}H NMR (300 MHz, CD$_3$OD & 3 drops of DMSO-d$_6$): δ 3.28 (dd, J = 13.8, 8.2 Hz, 1H), 3.38 (dd, J = 13.8, 3.5 Hz, 1H), 4.81 (dd, J = 8.2, 3.5 Hz, 1H), 7.25-7.45 (m, 5H); HRMS calcd for C$_9$H$_{13}$N$_3$O 180.1137 (M + H)$^+$, obsd 180.1131.

(-)-β-Guanyl-meta-octopamine (1e)

32% yield after recrystallization from ethanol/water : mp 225-227°C; $[\alpha]_D^{23}$ -28° in 50% aqueous MeOH; ^{1}H NMR (300 MHz, CD$_3$OD & 3 drops of DMSO-d$_6$): δ 3.30 (dd, J = 13.9, 8.0 Hz, 1H), 3.38 (dd, J = 13.9, 3.7 Hz, 1H), 4.81 (dd, J = 8.0, 3.7 Hz, 1H), 6.69 (ddd, J = 7.8, 2.4, 1.0 Hz, 1H), 6.70-6.89 (m, 2H), 7.16 (t, J = 7.8 Hz, 1H); HRMS calcd for C$_9$H$_{13}$N$_3$O$_2$ 196.1086 (M + H)$^+$, obsd 196.1089.

4-Methoxyphenethylguanidine sulfate (1f)

74% yield after recrystallization from water: mp 181-182°C (lit.46 183-184°C, lit.[47] 210-211°C); ^{1}H NMR (400 MHz, CD$_3$OD): δ 2.81 (t, J = 7.3 Hz, 2H), 3.36 (t, J = 7.3 Hz, 2H), 3.75 (s, 3H), 6.84 (d, J = 8.8 Hz, 2H), 7.17 (d, J = 8.8 Hz, 2H); HRMS calcd for C$_{10}$H$_{15}$N$_3$O 194.1293 (M + H)$^+$, obsd 194.1287.

3-Fluorophenethylguanidine sulfate (1g)

78% yield after recrystallization from ethanol/water: mp 188-189°C; ^{1}H NMR (400 MHz, CD$_3$OD): δ 2.90 (t, J = 7.3 Hz, 2H), 3.41 (t, J = 7.3 Hz, 2H), 6.94 (td, J = 8.4, 2.1Hz, 1H), 7.04 (dd, J = 10.0, 2.1 Hz, 1H), 7.09 (d, J = 7.8 Hz, 1H), 7.30 (td, J = 7.8, 2.1 Hz, 1H); HRMS calcd for C$_9$H$_{12}$FN$_3$ 181.1015 (M$^+$), obsd 181.1010.

4-Fluorophenethylguanidine sulfate (1h)

86% yield after recrystallization from water: mp 217-221°C; ^{1}H NMR (400 MHz, CD$_3$OD): δ 2.87 (t, J = 7.3 Hz, 2H), 3.38 (t, J = 7.3 Hz, 2H), 7.02 (d, J = 8.8 Hz, 2H), 7.28 (dd, J = 8.8, 5.4 Hz, 2H); HRMS calcd for C$_9$H$_{12}$FN$_3$ 182.1094 (M + H)$^+$, obsd 182.1091.

2-Fluorophenethylguanidine sulfate (1i)

0% yield after recrystallization from water: mp 185-186°C; ^{1}H NMR (400 MHz, CD$_3$OD): δ 2.94 (t, J = 7.2 Hz, 2H), 3.42 (t, J = 7.2 Hz, 2H), 7.06 (td, J = 8.4, 2.1Hz, 1H), 7.05 (td, J = 8.6, 1.2 Hz, 1H), 7.12 (td, J = 7.4, 1.2 Hz, 1H), 7.25 (m, 1H), 7.33 (td, J = 7.6, 1.6 Hz, 1H); HRMS calcd for C$_9$H$_{12}$FN$_3$ 181.1015 (M$^+$), obsd 181.1011.

General Procedure for the preparation of N,N'-bis(benzyloxycarbonyl)-N"-phenethylguanidines (3b, 3j, 3k)

To a solution of phenethylamine hydrochloride analog (3.54 mmol) and triethylamine (14.2 mmol) in dried DMF (20 mL) was added in portion 1,3-bis(benzyloxycarbonyl)-2-methyl-2-thiopseudourea (3.71 mmol) at room temperature. The reaction mixture was stirred overnight and then diluted with ethyl acetate (60 mL). The resulting solution was washed with saturated $NaHCO_3$ solution (80 mL) and extracted with ethyl acetate (2×100 mL). The combined extracts were dried over anhydrous Na_2SO_4 and concentrated under reduced pressure. The residue was flash-chromatographed on silica gel, eluting a mixture of ethyl acetate in hexane to afford N,N'-bis(benzyloxycarbonyl)-N"-3-hydroxyphenethylguanidine.

N,N'-Bis(benzyloxycarbonyl)-N"-3-hydroxyphenethylguanidine (3b)

99% yield after flash-chromatography using a 20-30% ethyl acetate/hexane gradient: mp 130-132°C; ^1H NMR (300 MHz, DMSO-d_6): δ 2.73 (t, J = 7.0 Hz, 2H), 3.53 (q, J = 7.0 Hz, 2H), 5.05 (s, 2H), 5.20 (s, 2H), 6.59-6.64 (m, 3H), 7.07 (t, J = 7.7 Hz, 1H), 7.30-7.43 (m, 10H), 8.44 (t, J = 5.6 Hz, 1H), 9.30 (s, 1H), 11.60 (s, 1H); HRMS calcd for $C_{25}H_{25}N_3O_5$ 470.1692 $(M + Na)^+$, obsd 470.1691.

N,N'-Bis(benzyloxycarbonyl)-N"-4-fluoro-3-hydroxyphenethylguanidine (3j)

97% yield after flash-chromatography using a 20-30% ethyl acetate/hexane gradient: mp 112-115°C; ^1H NMR (300 MHz, DMSO-d_6): δ 2.72 (t, J = 7.0 Hz, 2H), 3.51 (q, J = 6.7 Hz, 2H), 5.05 (s, 2H), 5.20 (s, 2H), 6.59-6.63 (m, 1H), 6.80 (dd, J = 8.5, 1.3 Hz, 1H), 7.02 (dd, J = 11.4, 8.5 Hz, 1H), 7.30-7.41 (m, 10H), 8.44 (t, J = 5.6 Hz, 1H), 9.75 (s, 1H), 11.61 (s, 1H); HRMS calcd for $C_{25}H_{24}FN_3O_5$ 488.1598 $(M + Na)^+$, obsd 488.1604.

N,N'-Bis(benzyloxycarbonyl)-N"-6-fluoro-3-hydroxyphenethylguanidine (3k)

100% yield after flash-chromatography using a 20-30% ethyl acetate/hexane gradient: mp 133-135°C; ^1H NMR (300 MHz, DMSO-d_6): δ 2.78 (t, J = 7.0 Hz, 2H), 3.54 (q, J = 6.6 Hz, 2H), 5.05 (s, 2H), 5.20 (s, 2H), 6.58-6.66 (m, 2H), 6.93(t, J = 9.2 Hz, 1H), 7.29-7.42 (m, 10H), 8.48 (t, J = 5.5 Hz, 1H), 9.32 (s, 1H), 11.61 (s, 1H); HRMS calcd for $C_{25}H_{24}FN_3O_5$ 488.1598 $(M + Na)^+$, obsd 488.1594.

N,N'-Bis(benzyloxycarbonyl)-N"-4-hydroxybenzylguanidine

100% yield after flash-chromatography using a 30% ethyl acetate/hexane gradient: mp 82-83°C; ^1H NMR (300 MHz, DMSO-d_6): δ 4.42 (t, J = 5.6 Hz, 2H), 5.04 (s, 2H), 5.20 (s, 2H), 6.71 (d, J = 8.5 Hz, 2H), 7.13 (d, J = 8.5 Hz, 2H), 7.30-7.43 (m, 10H), 8.48 (t, J = 5.6 Hz, 1H), 9.36 (s, 1H), 11.59 (s, 1H); HRMS calcd for $C_{24}H_{23}N_3O_5$ 456.1535 $(M + Na)^+$, obsd 456.1524.

General Procedure for the preparation of phenethylguanidines (1b, 1j & 1k) via Hydrogenolysis

The N,N'-bis(benzyloxycarbonyl)-N"-3-hydroxyphenethylguanidine (1.54 g, 3.44 mmol) was dissolved in ethyl acetate (10 mL) and methanol (30 mL) and 10% palladium on activated carbon (300 mg) was added. The mixture was hydrogenated at 40 p.s.i. for 5 hours. After filtration through the Celite pad, the solution was concentrated under reduced pressure to afford 3-hydroxyphenethylguanidine (559 mg, 3.12 mmol, 91% yield) as a viscous oil, which was used for the next step without further purification. To a solution of 3-hydroxyphenethylguanidine (412 mg, 2.30 mmol) in ethanol (10 mL) was added dropwise a solution of 0.505 N H_2SO_4 in H_2O (2.28 mL, 1.15 mmol). After the mixture was stirred for 5 min, a solution was concentrated under reduced pressure. The crude solid product was

recrystallized from ethanol to afford 409 mg (78%) of 3-hydroxyphenethylguanidine sulfate **1b** as a white solid.

3-Hydroxyphenethylguanidine sulfate[48] (1b)

78% yield after recrystallization from ethanol: mp 185-187°C; ^{1}H NMR (400 MHz, CD_3OD & 3 drops of DMSO-d_6): δ 2.80 (t, J = 7.2 Hz, 2H), 3.38 (t, J = 7.2 Hz, 2H), 6.64 (td, J = 7.8, 1.5 Hz, 1H), 6.72 (d, J = 7.8 Hz, 1H), 6.73 (s, 1H), 7.11 (t, J = 7.8 Hz, 1H); HRMS calcd for $C_9H_{13}N_3O$ 180.1137 (M + H)$^+$, obsd 180.1136.

4-Fluoro-3-hydroxyphenethylguanidine sulfate (1j)

63% yield after recrystallization from ethanol: mp 178-183°C; ^{1}H NMR (400 MHz, CD_3OD & 3 drops of DMSO-d_6): δ 2.84 (t, J = 7.0 Hz, 2H), 3.40 (t, J = 7.0 Hz, 2H), 6.67 (m, 1H), 6.87 (dd, J = 8.5, 2.0 Hz, 1H), 6.95 (dd, J = 11.1, 8.5 Hz 1H); HRMS calcd for $C_9H_{12}FN_3O$ 198.1043 (M + H)$^+$, obsd 198.1037.

6-Fluoro-3-hydroxyphenethylguanidine sulfate (1k)

82% yield after recrystallization from ethanol: mp 215-216°C; ^{1}H NMR (400 MHz, CD_3OD & 3 drops of DMSO-d_6): δ 2.84 (t, J = 7.0 Hz, 2H), 3.40 (t, J = 7.0 Hz, 2H), 6.62 (td, J = 9.0, 3.5 Hz, 1H), 6.78 (dd, J = 6.2, 3.5 Hz, 1H), 6.88 (t, J = 9.0 Hz 1H); HRMS calcd for $C_9H_{12}FN_3O$ 190.1043 (M + H)$^+$, obsd 198.1038.

4-Hydroxybenzylguanidine sulfate (5)

69% yield after recrystallization from ethanol: mp 255-257°C (lit.49 260-262°C); ^{1}H NMR (400 MHz, CD_3OD & 3 drops of DMSO-d_6): δ 2.84 (t, J = 7.0 Hz, 2H), 3.40 (t, J = 7.0 Hz, 2H), 6.62 (td, J = 9.0, 3.5 Hz, 1H), 6.78 (dd, J = 6.2, 3.5 Hz, 1H), 6.88 (t, J = 9.0 Hz 1H); HRMS calcd for $C_9H_{12}FN_3O$ 190.1043 (M + H)$^+$, obsd 198.1038.

Radiosynthesis of ^{11}C-labeled Phenethylguanidines

The radiosynthesis of ^{11}C-labeled phenethylguanidines ([^{11}C]**1a-m**) was achieved with [^{11}C] cyanogen bromide as the labeling reagent, based on previously described methods with some modifications.[29] No-carrier-added [^{11}C]CO_2 was prepared by proton bombardment of a nitrogen gas target [^{14}N(p,α)^{11}C], and catalytically reduced with hydrogen over a nickel catalyst at 385°C to form [^{11}C]CH_4. [^{11}C]CH_4 was mixed with ammonia and passed over a platinum catalyst held at 950°C to convert [^{11}C]CH_4 into [^{11}C]HCN, which was then passed through a quartz glass tube containing 0.4 g PyBr$_3$ to form [^{11}C]CNBr. While the conversion rate of [^{11}C]CO_2 to [^{11}C]CH_4 was >99%, conversion rates of [^{11}C]CH_4 to [^{11}C]HCN were variable, ranging from 47-85%. Starting quantities of [^{11}C]CNBr were estimated to range from 550-1000 mCi. In a 1.0 mL reaction vial, 1.0-1.5 mg of phenethylamine precursor as the free base or hydrochloride salt was dissolved in 0.25 mL of borate buffer (pH 8.0). [^{11}C]CNBr was collected in the reaction vial at room temperature in N_2 carrier (30 mL/min) until radioactivity in the vial had peaked (~ 3.5 min). The resulting mixture was heated at 80-85°C for 5 min and then cooled to about 40°C. After adding 0.25 mL of 35% NH_4Br in 25% NH_4OH to the reaction vial, the vial was sealed and heated at 130-135°C for 5 min to yield the desired [^{11}C] phenethylguanidine. The mixture was cooled to ambient temperature and then injected onto a Phenomenex Synergi 4μ Hydro RP column, 50 × 4.6 mm or 150 × 4.6 mm, eluting with 0.1 M ammonium acetate buffer or 60 mM sodium phosphate buffer with 0-10% ethanol. Column effluent was monitored for radioactivity and UV absorbance (224 or 241 nm). Retention times (R_t) ranged from 4.0 to 9.5 min at flow rates of 1.0 to 3.0 mL/min depending upon the differing polarities of the radiotracers. Corrected radiochemical yields were 2.5-6% (relative to [^{11}C]CO_2 produced), with specific activities of >500 Ci/mmol at end-of-synthesis (EOS).

Radiochemical and chemical purities were >98%. For most compounds, 25 - 60 mCi of activity was obtained at EOS, with synthesis times of 35-40 min.

Radiosynthesis of [^{11}C]HED and [^{11}C]EPI

[^{11}C]HED was synthesized by N-methylation of (-)-metaraminol as the free base, using previously described methods [14] with a few modifications. Briefly, [^{11}C]methyl triflate[50] in a N_2 carrier gas stream was bubbled at room temperature through 0.25 mL of dimethyl formamide (DMF) containing 1.0 mg of (-)-metaraminol until the radioactivity trapped in the reaction vial reached a maximum (~ 4 min). Because of the high reactivity of [^{11}C]methyl triflate, the reaction to form HED is extremely rapid and no heating of the reaction vial is necessary. HED was purified using HPLC (Phenomenex Partisil 10 μm SCX 4.6×250 mm column; mobile phase 60 mM NaH_2PO_4 monohydrate; flow rate 2.0 mL/min; R_t ~ 6 min). Total synthesis time, including HPLC purification and product formulation was ~ 35 min. Corrected radiochemical yields were 20-25%, with radiochemical purity >98% and specific activity >500 Ci/mmol. [^{11}C]EPI was synthesized under comparable conditions, except the [^{11}C]methyl triflate was passed through 0.25 mL dimethyl sulfoxide (DMSO) containing 1.0 mg of (-)-norepinephrine as the free base. HPLC purification conditions were the same as used for [^{11}C]HED except the mobile phase was 25 mM NaH_2PO_4 monohydrate; flow rate 3.0 mL/min; R_t ~ 6 min). Corrected radiochemical yields, radiochemical purities, and specific activities were comparable to those achieved with [^{11}C]HED.

Animal Care

The care of all animals used in this study was done in accordance with the Animal Welfare Act and the National Institutes of Health's *Guide for the Care and Use of Laboratory Animals*.[51] Animal protocols were approved by the University Committee on Use and Care of Animals (UCUCA) at the University of Michigan.

Isolated rat heart studies

Hearts from male Sprague-Dawley rats (225 - 500 g) were perfused under moderate workload conditions (7.3 mmHg preload, 73 mmHg afterload) using a working heart preparation based on the system of Taegtmeyer et al.[52] Two separate perfusion circuits were used in parallel, connected to the left atrial cannula with a 3-way connector to allow for rapid switching from one perfusion circuit to the other. The perfusion medium was Krebs-Henseleit (KH) bicarbonate buffer (118 nM NaCl, 4.7 mM KCl, 2.55 mM $CaCl_2$, 1.2 mM $MgSO_4$, 1.2 mM $K_2H_2PO_4$, and 25 mM $NaHCO_3$) containing 5 mM glucose and oxygenated with a 95% O_2/5% CO_2 gas mixture. Corticosterone (54 μM) was added to the perfusate to block extraneuronal uptake (uptake-2) of the radiotracers into the rat myocardium.[30]

Radioactivity in the heart was measured externally using a pair of cesium fluoride (CsF) scintillation detectors (Crismatec 51Y51; Saint-Gobain, Nemours, France), with the front faces of the two CsF detectors directly opposing each other and the heart centered between them. Each detector was enclosed in a large cylindrical lead collimator (2 cm wall thickness, 25 cm long) to minimize detected counts originating from radioactive sources outside the heart. Two coincidence detection circuits were established between the detectors using standard Nuclear Instrumentation Module (NIM) electronic modules. One circuit measured total coincident events between the two detectors (true + random coincident events), and the second measured only random coincident events. A computer-driven data acquisition system interfaced to the NIM-module coincidence circuits was used to acquire and record the whole-heart radioactivity data throughout the study.[37]

Hearts were initially perfused for a 30 min stabilization period using KH buffer in the first of the two perfusion circuits. During this time, the [^{11}C]-labeled tracer being studied was added

to 1.0 L of KH buffer circulating in the second perfusion circuit and allowed to mix for several minutes. Three 1.0 mL aliquots were then drawn from the second perfusion circuit and counted in a gamma counter (Perkin-Elmer MINAXI AutoGamma 5500) to determine the radioactivity concentration in the perfusate (C_p). Depending on the radiotracer being studied, radioactivity concentrations of 2.0 - 12.0 μCi/mL perfusate were used. After initiating data acquisition from the CsF detectors, the heart was rapidly switched to the second perfusion circuit to begin a constant infusion of the [^{11}C]-labeled tracer. After 10 min of constant infusion, the heart was switched back to the first perfusion circuit for 120 min to study clearance of the tracer from the heart.

The acquired whole-heart radioactivity data (counts per second; cps) at each time point were converted to an 'apparent distribution volume' (ADV; mL perfusate/g wet), by dividing by the perfusate radioactivity concentration C_p (μCi/mL perfusate), the external detection system calibration factor Z_{calib} (cps/μCi), and the measured wet mass of the heart M_w (g wet). Neuronal uptake rates of the radiotracers (K_{up}; mL perfusate/min/g wet) were calculated by fitting the ADV data between $t = 1$ min and $t = 4$ min of the 10 min constant infusion phase of the experiment to a line. Clearance rates were estimated by fitting the ADV data during the clearance phase of the study to multiple exponential decay processes. The exponential clearance rate constants (λ_i) were used to calculate corresponding clearance half-times ($T_{1/2} = \ln 2/\lambda_i$). The slowest estimated rate, associated with clearance from sympathetic neurons, is the rate reported for each compound.

Tissue Distribution Studies in Rat

Sprague-Dawley rats (200-225 g) were purchased from Charles River Laboratories, Inc., Wilmington, MA. For each radiotracer evaluated, five rats under light ether anesthesia received bolus tail-vein injections of 50 - 350 μCi of tracer in 0.05-0.10 mL of isotonic 60 mM sodium phosphate buffer, pH 4.5. Rats were killed by decapitation while under anesthesia at 30 min after tracer injection. Organs and blood samples were quickly removed from the rat carcasses and placed in previously weighed tubes. Tubes were weighed again to determine tissue masses and then counted in a gamma-counter (MINAXI Auto-Gamma 5500; Perkin-Elmer, Wellesley, MA). Gamma-counter data were corrected for radioactive decay and normalized to tissue mass to determine radiotracer tissue concentrations, expressed as percentage injected dose/g tissue (%ID/g).

Cardiac PET Imaging Studies

Cardiac PET studies were performed in rhesus macaque monkeys using a microPET P4 Primate scanner (Siemens/CTI Concorde Microsystems, Knoxville, TN). The monkey was anesthetized with isoflurane, intubated, and the tail shaved and disinfected for placement of a percutaneous angiocatheter. Opthalmic ointment was administered in the eyes and the animal placed on a recirculating water blanket on the scanner bed to maintain body temperature. After positioning the monkey in the scanner gantry, a 20 min transmission scan was acquired using a rotating ^{68}Ga source to generate attenuation correction data. Next, 5 - 6 mCi of radiotracer was injected via the catheter. Starting just before tracer injection, emission data from the PET scanner was collected in list-mode for 60 min. The list-mode PET data were rebinned into a 15-frame dynamic sequence (4×30 s, 3×60 s, 2×150 s, 2×300 s, 4×600 s). Images were reconstructed using an OSEM/3D-MAP reconstruction algorithm. Regions-of-interest were drawn on the left ventricle wall (LV), left ventricle chamber (blood) and liver to generate time-activity curves for each tissue from the dynamic PET images.

PET Imaging Studies of Adrenergic Tumors

Rat pheochromocytoma cells (PC12) were obtained from ATCC (Manassas, VA) and cultured under conditions recommended by ATCC. Athymic BALB/c *nu/nu* mice (*n* = 4, Charles River,

Wilmington, MA), 4-6 weeks old, were injected *s.c.* with 2.0 - 2.5 $\times$ 10^6 PC12 cells in 100 µL PBS in their left abdominal flank. After 4-5 weeks, when PC12 xenografts were 10-20 mm diameter and body weights were 23-25 g, PET imaging studies were performed using a microPET R4 Rodent scanner (Siemens/CTI Concorde Microsystems, Knoxville, TN). Anesthesia was induced with 5% isoflurane and maintained during the study using 2% isoflurane. The mice were placed on a recirculating water blanket on the scanner bed to maintain body temperature, and ophthalmic ointment was administered in the eyes. A 20 min transmission scan was acquired using a rotating ^{68}Ga source to generate attenuation correction data. Next, 0.3-0.4 mCi of radiotracer was injected via one of the catheters. The list-mode PET data were rebinned into a 12-frame dynamic sequence (5×120 s, 4×300 s, 3×600 s,. Images were reconstructed using an OSEM/3D-MAP reconstruction algorithm.

Supplementary Material

Refer to Web version on PubMed Central for supplementary material.

Acknowledgments

References

(1). Wieland DM, Wu J, Brown LE, Mangner TJ, Swanson DP, et al. Radiolabeled adrenergic neuron-blocking agents: adrenomedullary imaging with [^{131}I]iodobenzylguanidine. J. Nucl. Med 1980;21:349–353. [PubMed: 7381563]

(2). Sisson JC, Frager MS, Valk TW, Gross MD, Swanson DP, et al. Scintigraphic localization of pheochromocytoma. N. Engl. J. Med 1981;305:12–17. [PubMed: 7231514]

(3). Wieland DM, Mangner TJ, Inbasekaran MN, Brown LE, Wu J. Adrenal medulla imaging agents: a structure-distribution relationship study of radiolabeled aralkylguanidines. J. Med. Chem 1984;27:149–155. [PubMed: 6694163]

(4). Tobes MC, Jaques S, Wieland DM, Sisson JC. Effect of uptake-one inhibitors on the uptake of norepinephrine and metaiodobenzylguanidine. J. Nucl. Med 1985;26:897–907. [PubMed: 3162008]

(5). Bönisch H, Harder R. Binding of ^{3}H-desipramine to the neuronal noradrenaline carrier of rat phaeochromocytoma cells (PC-12 cells). Naunyn-Schmiedeberg's Arch. Pharmacol 1986;334:403–411.

(6). Lode HN, Bruchelt G, Sietz G, Gebhardt S, Gekeler V, et al. Reverse transcriptase-polymerase chain reaction (RT-PCR) analysis of monoamine transporters in neuroblastoma cell lines: correlations to meta-iodobenzylguanidine (MIBG) uptake and tyrosine hydroxylase gene expression. Eur. J. Cancer 1995;31A:586–590. [PubMed: 7576974]

(7). Wieland DM, Brown LE, Rogers WL, Worthington KC, Wu J-L, et al. Myocardial imaging with a radioiodinated norepinephrine storage analog. J. Nucl. Med 1981;22:22–31. [PubMed: 7452352]

(8). Flotats A, Carrió I. Cardiac neurotransmission SPECT imaging. J. Nucl. Cardiol 2004;11:587–602. [PubMed: 15472644]

(9). DeGrado TR, Zalutsky MR, Vaidyanathan G. Uptake mechanisms of meta-[^{123}I] iodobenzylguanidine in isolated rat heart. Nucl. Med. Biol 1995;22:1–12. [PubMed: 7735158]

(10). Nakajo M, Shimabukuro K, Yoshimura H, Yonekura R, Nakabeppu Y, et al. Iodine-131 metaiodobenzylguanidine intra- and extravesicular accumulation in the rat heart. J. Nucl. Med 1986;27:84–89. [PubMed: 3941369]

(11). Erickson JD, Schäfer MKH, Bonner TI, Eiden LE, Weihe E. Distinct pharmacological properties and distribution in neurons and endocrine cells of two isoforms of the human vesicular monoamine transporter. Proc. Natl. Acad. Sci 1996;93:5166–5171. [PubMed: 8643547]

(12). Wieland DM, Rosenspire KC, Hutchins GD, Van Dort M, Rothley JM, et al. Neuronal mapping of the heart with 6-[^{18}F]fluorometaraminol. J. Med. Chem 1990;33:956–964. [PubMed: 2308146]

(13). Goldstein DS, Chang PC, Eisenhofer G, Miletich R, Finn R, et al. Positron emission tomographic imaging of cardiac sympathetic innervation and function. Circulation 1990;81:1606–1621. [PubMed: 2331769]

(14). Rosenspire KC, Haka MS, Van Dort ME, Jewett DM, Gildersleeve DL, et al. Synthesis and preliminary evaluation of carbon-11-meta-hydroxyephedrine: A false transmitter agent for heart neuronal imaging. J. Nucl. Med 1990;31:1328–1334. [PubMed: 2384800]

(15). Chakraborty PK, Gildersleeve DL, Jewett DM, Toorongian SA, Kilbourn MR, et al. High yield synthesis of high specific activity *R*-(-)-[^{11}C]epinephrine for routine PET studies in humans. Nucl. Med. Biol 1993;20:939–944. [PubMed: 8298573]

(16). Del Rosario RB, Jung Y-W, Chakraborty PK, Sherman PS, Wieland DM. Synthesis and preliminary evaluation of [C-11] phenylephrine for mapping heart neuronal function. Nucl. Med. Biol 1996;23:611–616. [PubMed: 8905825]

(17). Loc'h C, Mardon K, Valette H, Brutesco C, Merlet P, et al. Preparation and pharmacological characterization of 76Br-meta-bromobenzylguanidine (76Br-MBBG). Nucl. Med. Biol 1994;21:49–55. [PubMed: 9234263]

(18). Garg PK, Garg S, Zalutsky MR. Synthesis and preliminary evaluation of *para*- and *meta*-[^{18}F] fluorobenzylguanidine. Nucl. Med. Biol 1994;21:97–103. [PubMed: 9234270]

(19). Raffel DM, Wieland DM. Assessment of cardiac sympathetic nerve integrity with positron emission tomography. Nucl. Med. Biol 2001;28:541–559. [PubMed: 11516699]

(20). Bengel FM, Schwaiger M. Assessment of cardiac sympathetic neuronal function using PET imaging. J. Nucl. Cardiol 2004;11:603–616. [PubMed: 15472645]

(21). Raffel DM, Chen W, Sherman PS, Gildersleeve DL, Jung YW. Dependence of cardiac ^{11}C-meta-hydroxyephedrine retention on norepinephrine transporter density. J. Nucl. Med 2006;47:1490–1496. [PubMed: 16954558]

(22). Fielden R, Green AL. The effects of some aralkylguanidines in mice. Brit. J. Pharmacol 1965;24:408–417.

(23). Green AL, Fielden R, Bartlett DC, Cozens MJ, Eden RJ, et al. New norepinephrine-depleting agents. β-hydroxyphenethylguanidine and related compounds. J. Med. Chem 1967;10:1006–1008. [PubMed: 6056024]

(24). Costa E, Kunstman R, Gessa GL, Brodie BB. Structural requirements for bretylium and guanethidine-like activity in a series of guanidine derivatives. Life Sci 1962;3:75–80. [PubMed: 13881572]

(25). Konkel JT, Fan J, Jayachandran B, Kirk KL. Syntheses of 6-fluoro-*meta*-tyrosine and of its metabolites. J. Fluorine Chem 2002;115:27–32.

(26). Rathke B. Ueber Verbindungen des Schwefelharnstoffs. Ber. Dtsch. Chem. Ges 1884;17:297–309.

(27). Greenhill JV, Lue P. Amidines and guanidines in medicinal chemistry. Prog. Medicinal Chem 1993;30:203–326.

(28). Su W. A convenient synthesis of di-(benzyloxycarbonyl)-protected guanidines. Synth. Comm 1996;26:407–461.

(29). Westerberg G, Långström B. Synthesis of *meta*-iodobenzyl [^{11}C]guanidine. J. Labeled Compds. Radiopharm 1997;39:525–529.

(30). Salt PJ. Inhibition of noradrenaline uptake$_2$ in the isolated rat heart by steroids, clonidine and methoxylated phenylethylamines. Eur. J. Pharmacol 1972;20:329–340. [PubMed: 4643454]

(31). DeGrado TR, Hutchins GD, Toorongian SA, Wieland DM, Schwaiger M. Myocardial kinetics of carbon-11-meta-hydroxyephedrine: retention mechanisms and effects of norepinephrine. J. Nucl. Med 1993;34:1287–1293. [PubMed: 8326386]

(32). Nguyen NTB, DeGrado TR, Chakraborty P, Wieland DM, Schwaiger M. Myocardial kinetics of C-11 epinephrine in the isolated working rat heart. J. Nucl. Med 1997;38:780–785. [PubMed: 9170446]

(33). Musacchio JM, Kopin IJ, Weise VK. Subcellular distribution of some sympathomimetic amines and their β-hydroxylated derivatives in the rat heart. J. Pharmacol. Exp. Ther 1965;148:22–28. [PubMed: 14279180]

(34). Berry CR, DeGrado TR, Nutter F, Garg PK, Breitschwerdt EB, et al. Imaging of pheochromocytoma in 2 dogs using p-[^{18}F] fluorobenzylguanidine. Vet. Radiol. Ultrasound 2002;43:183–186. [PubMed: 11954815]

(35). Berry CR, Garg PK, Zalutsky MR, Coleman RE, DeGrado TR. Uptake and retention kinetics of *para*-fluorine-18-fluorobenzylguanidine in isolated rat heart. J. Nucl. Med 1996;37:2011–2016. [PubMed: 8970525]

(36). DeGrado TR, Zalutsky MR, Coleman RE, Vaidyanathan G. Effects of specific activity on *meta*-[^{131}I]iodobenzylguanidine kinetics in isolated rat heart. Nucl. Med. Biol 1998;25:59–64. [PubMed: 9466363]

(37). Raffel D, Loc'h C, Mardon K, Mazière B, Syrota A. Kinetics of the norepinephrine analog [Br-76]-*meta*-bromobenzylguanidine in isolated working rat heart. Nucl. Med. Biol 1998;25:1–16. [PubMed: 9466356]

(38). Law MP, Osman S, Davenport RJ, Cunningham VJ, Pike VW, et al. Biodistribution and metabolism of [N-methyl-^{11}C]-*m*-hydroxyephedrine in the rat. Nucl. Med. Biol 1997;24:417–424. [PubMed: 9290077]

(39). Carr EA, Carroll M, Counsell RE, Tyson JW. Studies of uptake of the bretylium analogue, iodobenzyltrimethylammonum iodide, by non-primate, monkey and human heart. Br. J. clin. Pharmacol 1979;8:425–432. [PubMed: 116669]

(40). Dae MW, De Marco T, Botvinick EH, O'Connell W, Hattner RS, et al. Scintigraphic assessment of MIBG uptake in globally denervated human and canine hearts -- implications for clinical studies. J. Nucl. Med 1992;33:1444–1450. [PubMed: 1634934]

(41). Glowniak J, Turner F, Gray L, Palac R, Lagunas-Solar M, et al. Iodine-123 metaiodobenzylguanidine imaging of the heart in idiopathic congestive cardiomyopathy and cardiac transplants. J. Nucl. Med 1989;30:1182–1191. [PubMed: 2661758]

(42). Eisenhofer G, Smolich JJ, Esler MD. Disposition of endogenous adrenaline compared to noradrenaline released by cardiac sympathetic nerves in the anaesthetized dog. Naunyn-Schmiedeberg's Arch. Pharmacol 1992;345:160–171.

(43). Raffel DM, Corbett JR, del Rosario RB, Gildersleeve DL, Chiao PC, et al. Clinical evaluation of carbon-11-phenylephrine: MAO sensitive marker of cardiac sympathetic neurons. J. Nucl. Med 1996;37:1923–1931. [PubMed: 8970507]

(44). Sisson JC, Shulkin BL. Nuclear medicine imaging of pheochromocytoma and neuroblastoma. Q. J. Nucl. Med 1999;43:217–223. [PubMed: 10568137]

(45). Braun CE. Preparation of some structurally related monoguanidines. J. Am. Chem. Soc 1933;55:1280–1284.

(46). Spickett, RGW.; Durant, GJ.; Willey, GL. Guanidines; Great Britain: 1966. p. 5

(47). Aroyan AA, Kocharyan SP. Synthesis of some amines, amidoximes, and derivatives of guanidine. Izvestiya Akademii Nauk Armyanskoi SSR Khimicheskie Nauki 1964;17:543–548.

(48). Sperry S, Crews P. Dihydrotubastrines: phenethylguanidine analogs from the Indo-Pacific marine sponge Petrosia cf. contignata. J. Nat. Prod 1998;61:859–861. [PubMed: 9644088]

(49). Lee H, Inbasekaran MN, Wieland DM, Sherman PS, Fisher SJ, et al. Development of a kit-form analog of metaiodobenzylguanidine. J. Nucl. Med 1986;27:256–267. [PubMed: 3712043]

(50). Jewett DM. A simple synthesis of [^{11}C]-methyl triflate. Appl. Radiat. Isot 1992;43:1383–1385.

(51). National Research Council. Guide for the Care and Use of Laboratory Animals. U.S. Department of Health and Human Services, National Institutes of Health; Bethesda, MD: 1985.

(52). Taegtmeyer H, Hems R, Krebs HA. Utilization of energy providing substrates in the isolated working rat heart. Biochem. J 1980;186:701–711. [PubMed: 6994712]
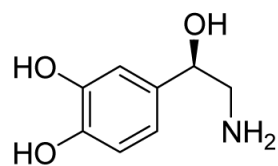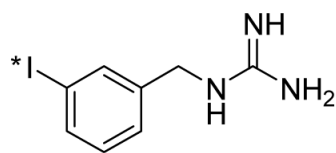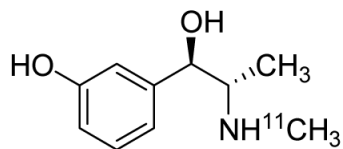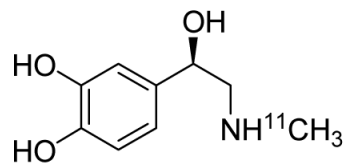
Figure 1.
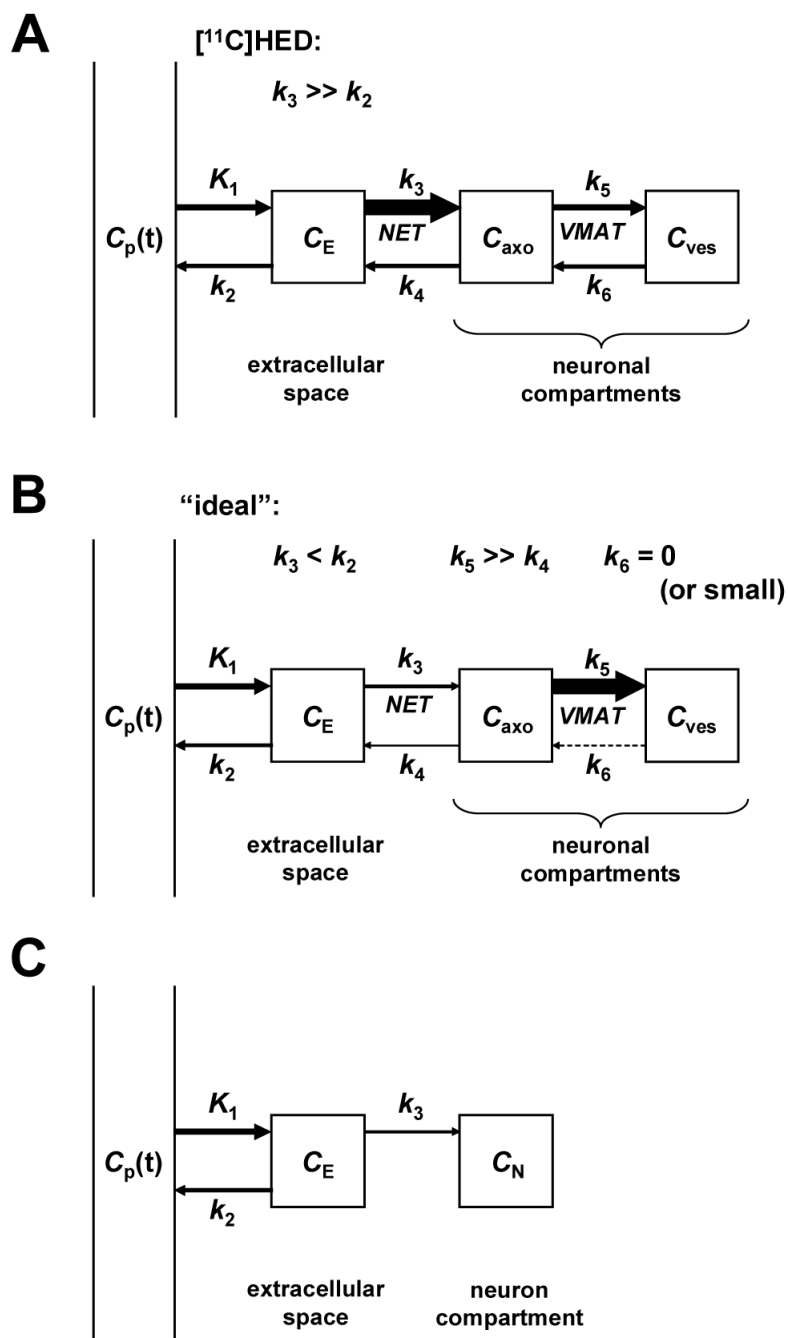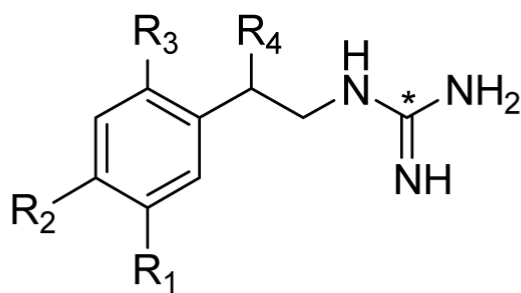Structures of norepinephrine and some clinically used sympathetic nerve imaging agents.

Figure 2.
A: Comprehensive compartmental model of [^{11}C]HED kinetics in the heart. Arrow thicknesses indicate relative magnitudes of rate constants. K_1 has units of mL/min/g; all other rate constants have units of min^{-1}. C_p = concentration in plasma; C_E = concentration in extracellular space; C_{axo} = concentration in neuronal axoplasm; C_{ves} = concentration in vesicles; NET = norepinephrine transporter; VMAT = vesicular monoamine transporter. **B**: Comprehensive compartmental model of a tracer with 'ideal' kinetic properties for kinetic modeling. **C**: Simplified compartmental model that could be used to analyze the myocardial kinetics of a PET tracer possessing the 'ideal' kinetic properties shown in **B**.

[¹¹C]1a-m

	R_1	R_2	R_3	R_4
a	H	H	H	H
b	OH	H	H	H
c	H	OH	H	H
d	H	H	H	(−)-OH
e	OH	H	H	(−)-OH
f	H	MeO	H	H
g	F	H	H	H
h	H	F	H	H
i	H	H	F	H
j	OH	F	H	H
k	OH	H	F	H
l	I	H	H	H
m	H	I	H	H

Figure 3.
General structure of [¹¹C]phenethylguanidines and compounds synthesized.
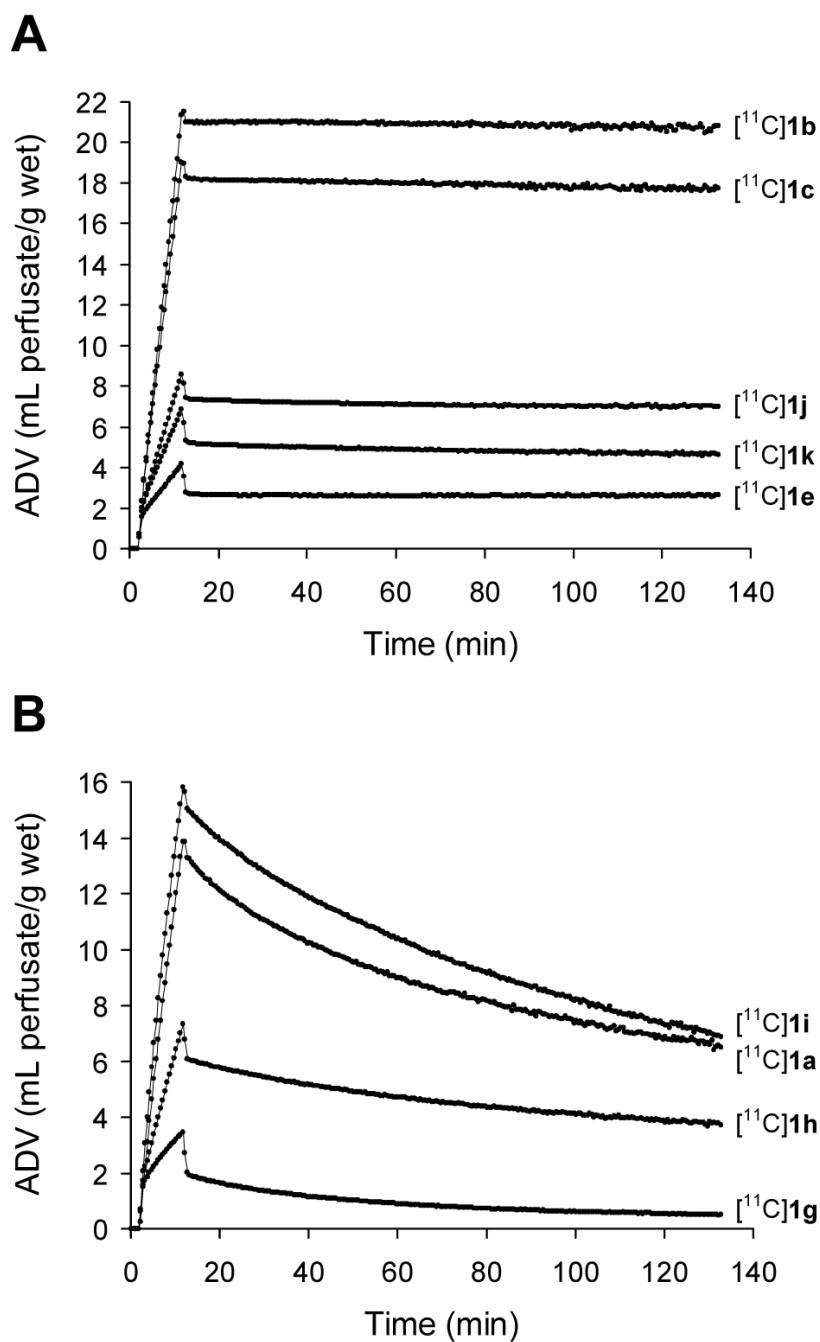
Figure 4.
Neuronal uptake and clearance kinetics of [^{11}C]phenethylguanidines in the isolated rat heart.
A: Five of the six compounds that exhibited long neuronal retention times. For clarity, compound [^{11}C]**1d** is not shown due to its similar kinetics with [^{11}C]**1k**. **B**: The unsubstituted reference compound [^{11}C]**1a** and the three analogs with a single ring fluoro-substitution.
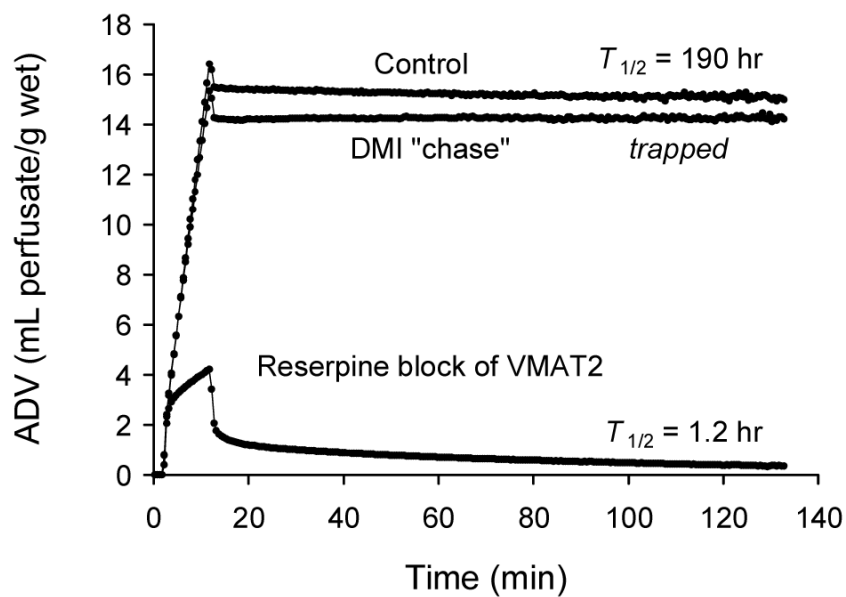
Figure 5.
Kinetics of [^{11}C]**1c** in the isolated rat heart under: (a) control conditions; (b) desipramine (DMI) chase to prevent neuronal reuptake during tracer clearance; and (c) reserpine block of vesicular storage.
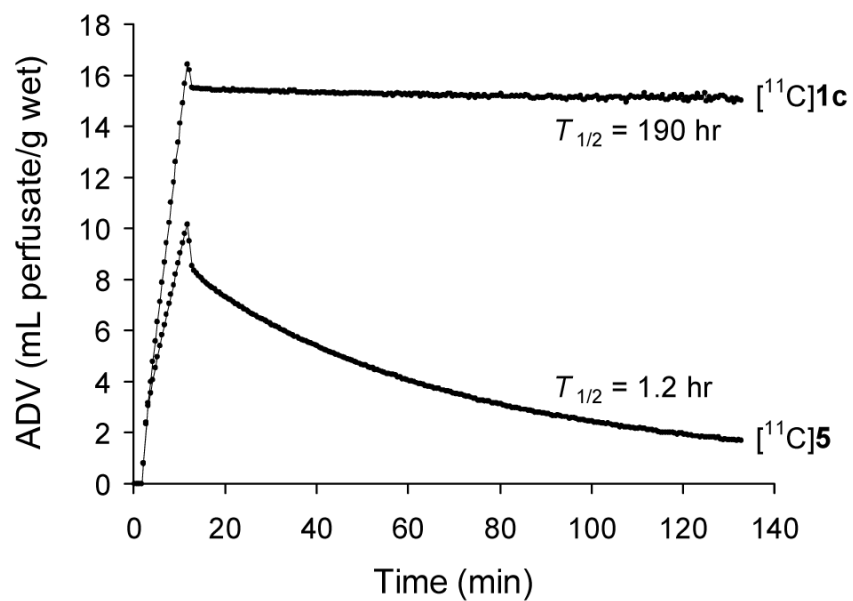
Figure 6.
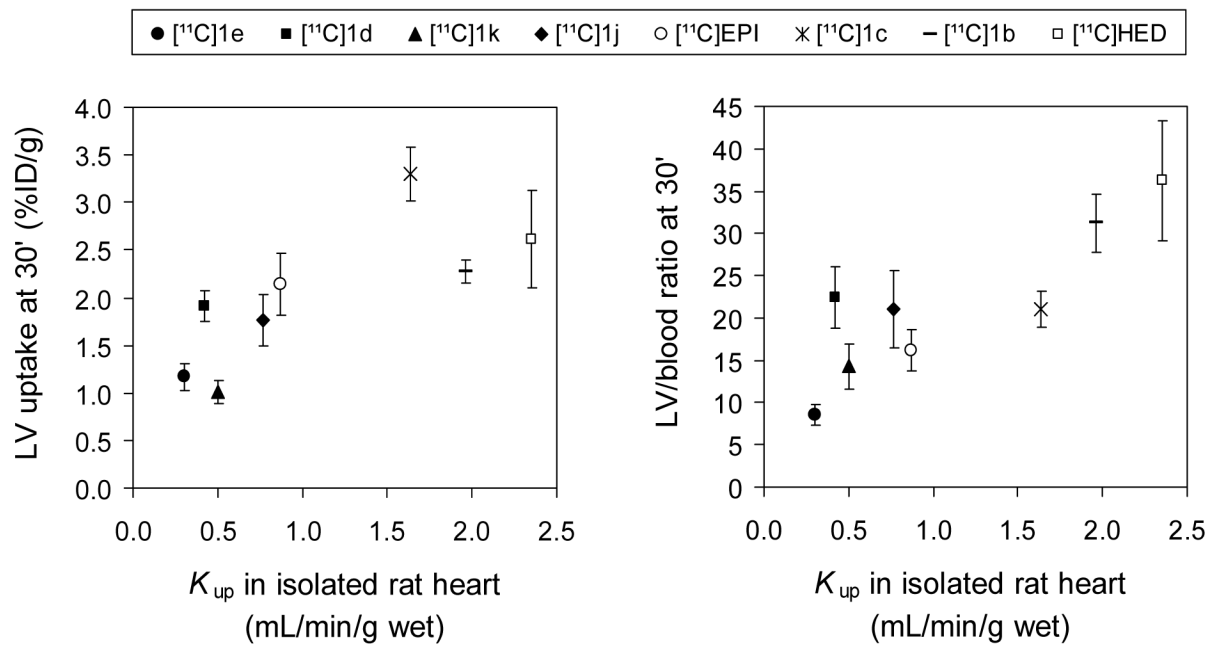Kinetics of [¹¹C]**1c** and its benzylguanidine analog [¹¹C]**5** in the isolated rat heart.

Figure 7.
Relationship between *in vivo* uptake of compounds in the left ventricle (LV) of the rat and neuronal uptake rates measured in the isolated rat heart (K_{up}).
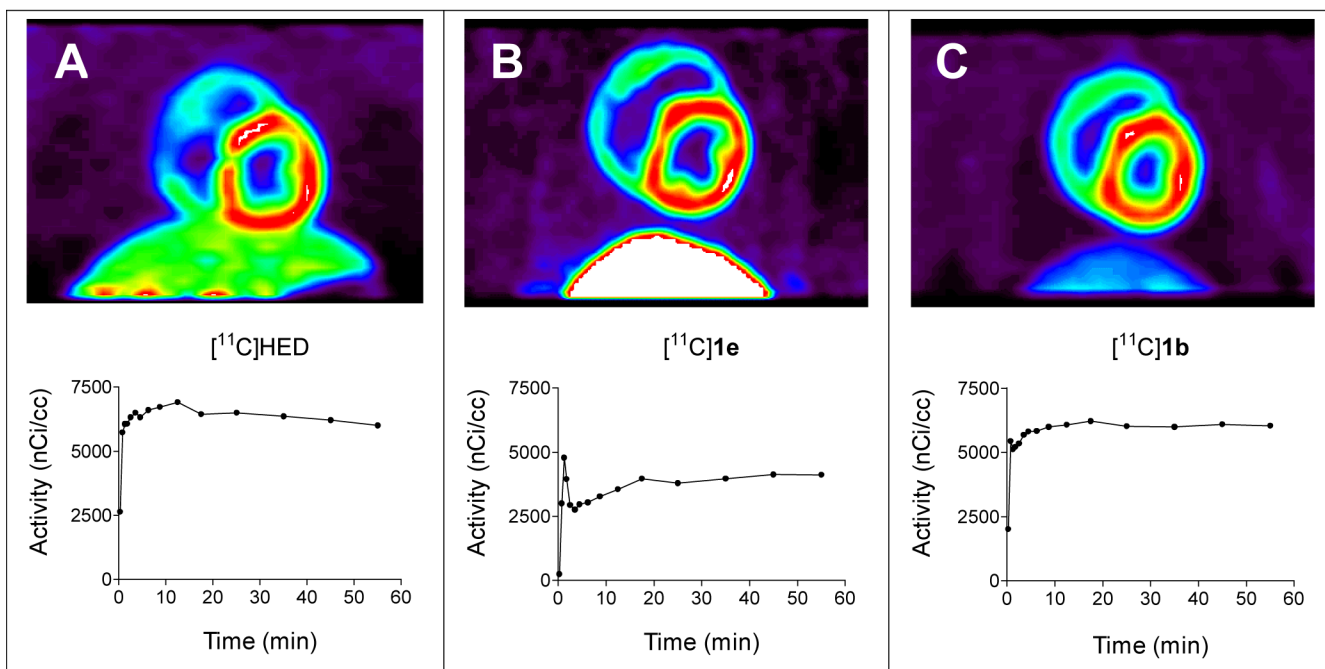
Figure 8.
Representative PET images (coronal slice) and corresponding myocardial kinetics of selected compounds in the rhesus macaque monkey. **A**: [^{11}C]HED, 5.4 mCi injected into a 5.3 kg monkey. **B**: [^{11}C]**1e**, 4.9 mCi injected into a 4.7 kg monkey. **C**: [^{11}C]**1b**, 4.8 mCi injected into a 5.8 kg monkey. The images are summed images of the data in the final 5 frames of the 15-frame dynamic sequence (15-60 min).
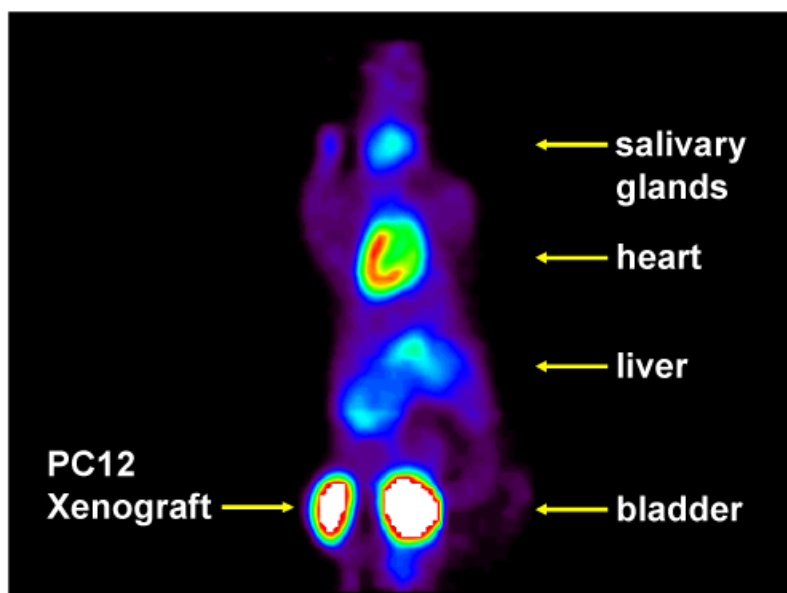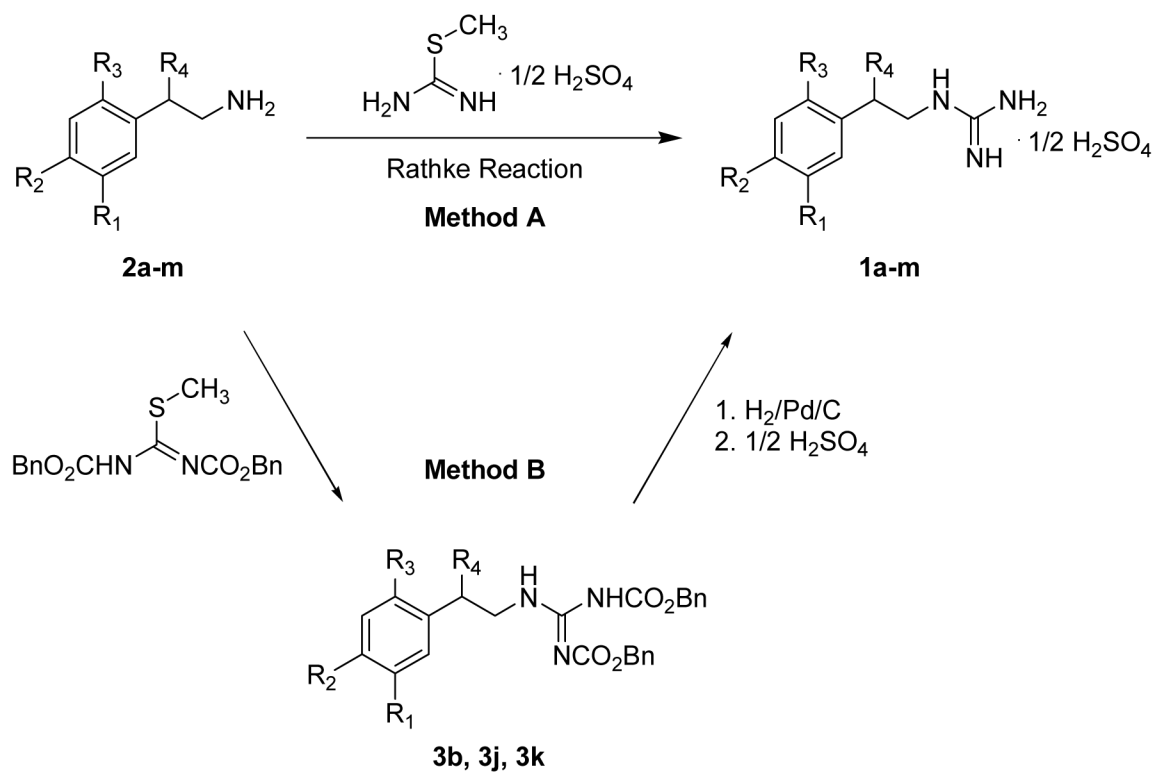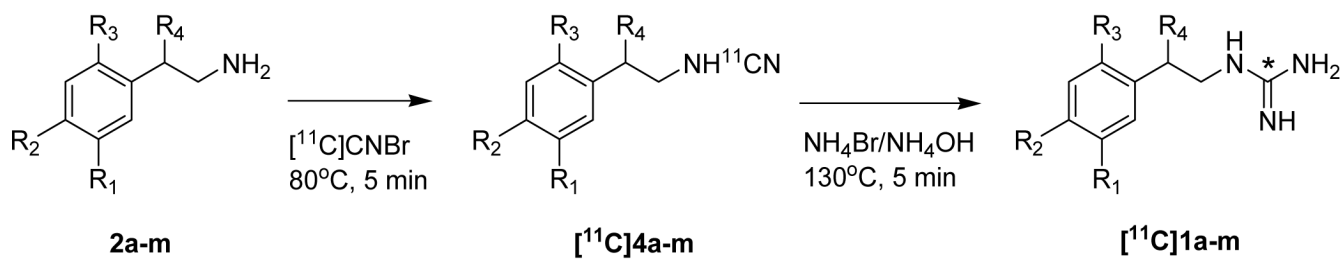
Figure 9.
PET image of [^{11}C]**1c** in a BALB/c *nu/nu* mouse with a rat pheochromocytoma (PC12) xenograft tumor in the left flank. A dose of 0.34 mCi was injected into the 25 g mouse. The image is a summed image of the data in the final 6 frames of the 12-frame dynamic sequence (15-60 min).
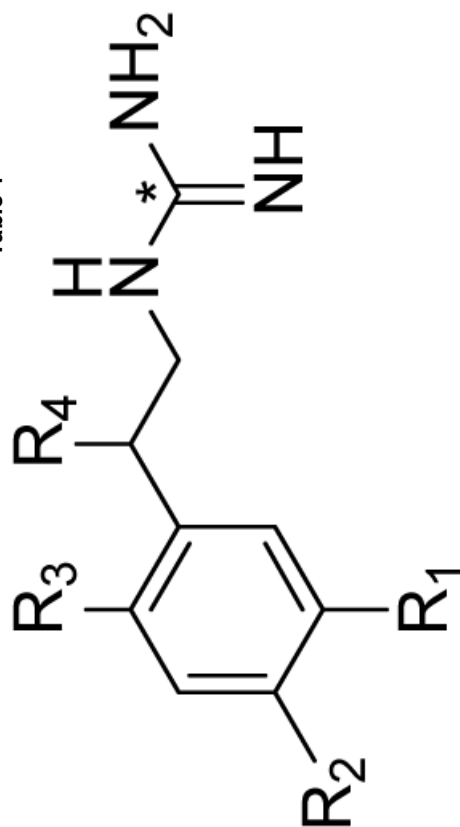
Scheme 1.

Scheme 2.

Table 1

Neuronal Uptake and Clearance Rates of [11C]Phenethylguanidines in Isolated Rat Heart[a]

compd	R1	R2	R3	R4	name	acronym	K_{up} (ml/min/g)	major clearance $T_{1/2}$ (hr)
[11C]1a	H	H	H	H	[11C]phenethylguanidine (PG)	PG	1.56	3.3
[11C]1b	OH	H	H	H	[11C]meta-hydroxy-PG	MHPG	1.96 ± 0.13	>102
[11C]1c	H	OH	H	H	[11C]para-hydroxy-PG	PHPG	1.64 ± 0.15	>45
[11C]1d	H	H	H	(-)-OH	[11C](-)-β-hydroxy-PG	BHPG	0.42	22
[11C]1e	OH	H	H	(-)-OH	N-[11C]guanyl-meta-octopamine	GMO	0.30 ± 0.02	>152
[11C]1f	H	MeO	H	H	[11C]para-methoxy-PG	PMPG	0.73	2.3
[11C]1g	F	H	H	H	[11C]meta-fluoro-PG	MFPG	0.24	1.9
[11C]1h	H	F	H	H	[11C]para-fluoro-PG	PFPG	0.63	4.4
[11C]1i	H	H	F	H	[11C]ortho-fluoro-PG	OFPG	1.76	2.3
[11C]1j	OH	F	H	H	[11C]para-fluoro-meta-hydroxy-PG	4F-MHPG	0.72 ± 0.05	>73
[11C]1k	OH	H	F	H	[11C]ortho-fluoro-meta-hydoxy-PG	6F-MHPG	0.49 ± 0.07	>20
[11C]1l	I	H	H	H	[11C]meta-iodo-PG	MIPG	1.10	2.4
[11C]1m	H	I	H	H	[11C]para-iodo-PG	PIPG	0.56	1.9

[a]For compounds with multiple determinations, K_{up} data are mean ± standard deviation (SD) and $T_{1/2}$ is the fastest measured clearance rate for $n = 5$ independent determinations. Coefficients of variation (SD/mean) for these ranged from 7-14%. Single determination values can be expected to be within this range. Extraneuronal uptake (uptake-2) was inhibited in all studies by adding 54 μM corticosterone to the perfusate.

Table 2

Tissue Concentrations of ^{11}C-labeled Compounds at $T = 30$ min in Rats [a]

compd	ventricle left	lung	liver	spleen	muscle	adrenal medulla	blood
[11C]HED	2.85 ± 0.42	0.40 ± 0.12	2.32 ± 0.25	1.31 ± 0.14	0.17 ± 0.02	0.72 ± 0.08	0.08 ± 0.01
[11C]EPI	2.14 ± 0.32	0.39 ± 0.05	1.95 ± 0.16	0.64 ± 0.02	0.22 ± 0.03	0.61 ± 0.18	0.13 ± 0.01
[11C]1b	2.28 ± 0.12	0.74 ± 0.15	0.89 ± 0.13	0.63 ± 0.16	0.07 ± 0.01	0.88 ± 0.15	0.07 ± 0.01
[11C]1c	3.30 ± 0.28	0.68 ± 0.16	0.84 ± 0.21	0.97 ± 0.06	0.14 ± 0.04	1.17 ± 0.16	0.16 ± 0.01
[11C]1d	1.91 ± 0.16	0.86 ± 0.11	3.91 ± 0.23	0.88 ± 0.07	0.10 ± 0.03	0.53 ± 0.07	0.09 ± 0.01
[11C]1e	1.17 ± 0.14	0.75 ± 0.10	2.71 ± 0.36	0.63 ± 0.10	0.07 ± 0.01	0.36 ± 0.06	0.14 ± 0.01
[11C]1j	1.77 ± 0.27	0.56 ± 0.15	1.22 ± 0.18	0.52 ± 0.10	0.07 ± 0.01	0.56 ± 0.21	0.08 ± 0.01
[11C]1k	1.01 ± 0.12	0.34 ± 0.06	0.92 ± 0.07	0.43 ± 0.12	0.06 ± 0.01	0.46 ± 0.07	0.07 ± 0.01

[a]Values are % injected dose/g; mean ± standard deviation of five determinations.